Defence Science Journal, Vol. 67, No. 2, March 2017, pp. 141-148, DOI : 10.14429/dsj.67.11177

Numerical Study of Dual band (MW/LW) IR Detector for Performance Improvement

P.K. Saxena

Tech Next Lab Private Limited, Lucknow – 226 003, India
E-mail: a.saxena@technextlab.com

ABSTRACT

In the present study, an extensive numerical analysis has been performed and an effort has been made to understand the underlying physics, which is presently unclear for researchers for development of third generation FPA infrared detectors based on HgCdTe material. To reduce technology development cost associated with dual band photodetector for operation at MWIR and LWIR regions, a 2D theoretical model has been proposed including all the relevant physics. The structure under present study considers back-to-back diode structures to detect simultaneous MW/LW operative wavelength by changing the biasing polarity of the diodes. The optimum electrical and optical outputs from dual band detector have been achieved through performing design of experiments. The coupled basic semiconductor equations including nonlinear continuity, transport and Poisson's equations have been solved to achieve electrical (I-V) characteristics under no bias condition and modern optics equations has been coupled to semiconductor equations to obtain optical characteristics. The quantum efficiency of both detectors has been computed and compared with experimental results. The computed results obtained on the basis of proposed model accurately matches with the experimental results reported by others researcher. The results exhibit the quantum efficiencies, QE_{MW}=95 per cent and QE_{LW}=74.5 per cent, respectively.

Keywords: Dual band; Infrared detector; Photodetector; EHP; Design of experiments

ABBREVIATIONS

SW	Short wavelength
MW	Medium wavelength
LW	Long wavelength
VLW	Very long wavelength
SWIR	Short wavelength infrared
MWIR	Medium wavelength infrared
LWIR	Long Wavelength infrared
VLWIR	Very long wavelength infrared
MCT	Mercury cadmium telluride
FPA	Focal plane array
GR	Generation recombination
TAT	Trap assisted tunnelling
BTB	Band to band tunnelling
DOE	Design of experiments
IR	Infrared
EHP	Electron hole pair
QE	Quantum efficiency

1. INTRODUCTION

The development of infrared detector has been started since 1940 especially for thermal imaging applications. The classification of infrared regions becomes possible due to availability of different advanced compound semiconductor materials. The infrared region has been classified as SW (1 µm - 2 µm), MW (3 µm - 5 µm), LW (8 µm - 12 µm) and VLW (> 12 µm) wavebands. Different materials systems have their significance for different IR transmission windows based on their material properties.

The development of high sensitivity infrared photo-detectors could be possible due to synthesis of mercury-cadmium-telluride (MCT) material during early 1960's. The material properties of HgCdTe have shown tremendous potential for operation starting from SWIR window to VLWIR window. The present MCT advance material growth technology enables it for different detectors designs applications. The MCT based IR detectors basically exploit for defense applications, thermal imaging, space applications, medical applications, environment monitoring and surveillance, and amongst other applications. The major recent applications of MCT based IR detector for development of astronomical systems.

The best suited IR windows for infrared imaging are MWIR (3 µm - 5 µm) and LWIR (8 µm - 12 µm) as the highest atmospheric transmission is possible through these two windows. For high sensitive IR imaging, the two IR windows require different conditions which depends on background signal, atmospheric transmission under diverse weather conditions, contrast etc factors.

MWIR window operations require higher contrast, clear weather, high humidity and high resolution conditions, while LWIR window operation favours much reduced background clutter (high temperature counter measure), better immunity to fog, dust, haze, and atmospheric turbulence. To achieve better choice ideal system performance with complex combination of above operating conditions requires dual band operation simultaneously.

Received : 01 January 2016, Revised : 16 January 2017
Accepted : 04 February 2017, Online published : 11 March 2017

Uni-colour MCT based photodetectors designs have been commercialised for MWIR and LWIR applications. Researchers are trying to develop multiband detectors which can detect multi wavelengths simultaneously. The multiband detectors show great potential for development of IR next level technology, in turn can reduce the fabrication cost associated with the technology and also easiness of operation. The dual band detector has been developed previously but suffered from bias selectivity issue i.e. separately selection of diode biasing is impossible simultaneously. The other issue associated with grown dual band detectors is optical crosstalk reducing the performance of the detector[1-12].

Few attempts have been performed by researchers to address the above problems associated with dual band detector technology. The recently published simulation analysis by Vallone[2], *et. al.* shows that 1D models are not feasible for dual band detection systems as several physical mechanisms inside the device can be defined through additional physics in other dimension as well. The 2D and 3D simulation study shows that the simulated results are more or less similar for both cases[2].

Researchers are trying is to reduce crosstalk effects within the structure consisting of two photodetectors back-to-back. A physics based complete model can quantitatively evaluate and explain the crosstalk associated with such complex structure. The physics based model can provide useful design guidelines to design engineers for minimisation of crosstalk effects and bias selectivity issue for development of third generation IR technology[3-4].

In this study, we have considered historical structure fabricated by Reine[13], *et al.* for model development and calibration purposes. The device under consideration consists of multilayer hetero-junction structures based on $Hg_{1-x}Cd_xTe$ with different mole fractions (x) for operation in two different IR windows. 2D cross sectional view of proposed structure under present study is as shown in Fig. 1(a) consisting of five different layers of MCT with varying mole-fraction and doping densities. A thin layer of HgCdTe, with bandgap energy higher than both adjacent MCT layers, has been sandwiched between two diodes for formation of barrier. The schematic energy bandgap diagram is as shown in Fig. 1(b), which is clearly showing the peak as barrier for adjacent layer's carriers[13].

In present structure design, we have neglected the contribution of substrate CdZnTe for growth of HgCdTe material, as in simulation study CdZnTe do not play any significant influence on the device characteristics. A 45 μm^2 × 8 μm^2 rectangular geometrical region with P-type $Hg_{0.55}Cd_{0.45}Te$ material with doping concentration 1×10^{23} /m^3 for cutoff wavelength 4.3 µm has been chosen as substrate including all relevant material parameters associated with HgCdTe material for particular mole fraction x. An 45 μm^2 × 8 μm^2 rectangular N-Type $Hg_{0.68}Cd_{0.32}Te$ with doping concentration 1×10^{21} /m^3 has been designed to making it hetero-junction IR detector for operation in MWIR (2 µm - 5 µm) window. An N-Type barrier layer with 45 μm^2 × 1 μm^2 rectangular shape has been designed with HgCdTe material with mole fraction x = 0.345 and doping density 1×10^{21} /m^3. The barrier layer works as a buffer layer for transport of charge carriers from N-type (x = 0.22) HgCdTe layer also for charge carriers for HgCdTe (with x = 0.225) layer.

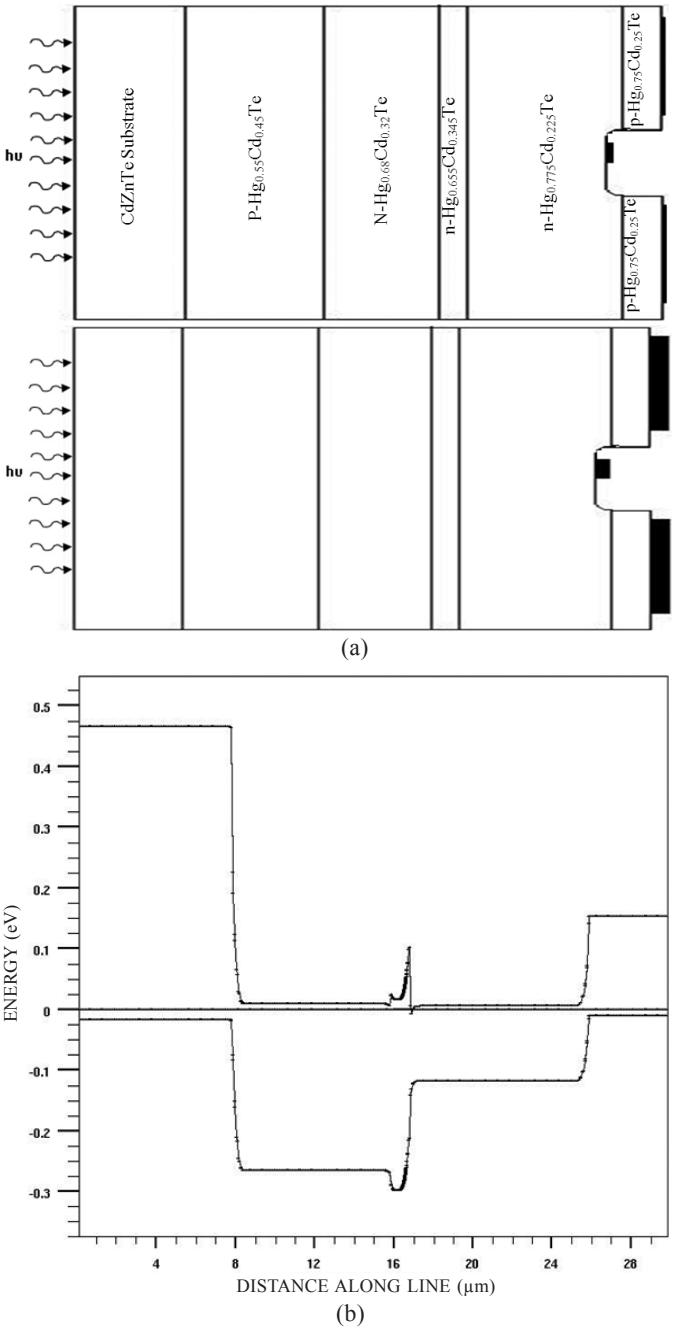

Figure 1. (a) Schematic diagram of dual band structure, and (b) Simulated energy band diagram.

An n-type layer of HgCdTe material for x = 0.225 is designed with 45×9 μm^2 rectangular shape and doping density 10^{21} / m^3. A p-type 45×4 μm^2 rectangular shape $Hg_{0.75}Cd_{0.25}Te$ with doping density 2.5×10^{23} /m^3 has been designed to make another p-n hetero-junction for operation in LWIR (8 µm - 12 µm). The p-type $Hg_{0.75}Cd_{0.25}Te$ layer has been etched out totally at middle of the layer for making common cathode electrode for both IR detector as the conductivity of all three n-N-N is same through the structure below cathode contact. The two anodes have been designed on top and bottom P- and p-type layer as shown in Fig. 1(a).

The schematic energy band diagram as shown in Fig. 1(b) demonstrate the two p-n hetero-structures with sandwiched barrier layer show the energy offset in the conduction ΔE_C and

valance band ΔE_V. The ground state degeneracy of conduction band g_c has been taken 2 while valance band degeneracy g_v has been taken 4. The energy offset in both bands is due to difference in electron affinities of different mole fraction of HgCdTe layers and doping concentration gradient. The classical energy band theory from Anderson, also justifies the band offset. The gradient in electrostatic potential ∇V and electron affinity $\nabla \div$ at barrier layer restricts transportation of carriers in form of electric potential. The electrons are essential transport current carriers as barrier offer less resistance in path of electrons transport as compared to hole transportation. The potential variation in Fig. 1(b) simply shows the band offset at each hetero-interface. The doping density profile play essential role in defining the barrier height at each hetero-interfaces[14-15].

The electrical characterisation of the designed structure has been done by solving the basic non linear decoupled equations, consists of continuity equation for both electrons and holes, carrier transport equations and Poisson equation with appropriate boundary conditions. Degenerate semiconductor and parabolic shape of conduction band have been taken into account for present numerical analysis. The commercial software from SILVACO® has been exploited for present numerical analysis. The designed structure has been optically characterised by coupling modern optics equation with the basic semiconductor equations. The absorption phenomenon is dependent on the imaginary part of refractive indices of different material with respect to incident wavelength[13].

The physical models associated with the designed structure include analytically uniform doping for all regions. For mobility model responsible for carriers transport, the concentration dependent ANALYTIC model has been chosen. Carrier lifetime modelling has been performed by taking into account AUGER, Shockley Read Hall (SRH), Trap assisted tunnelling (TAT) and band-to-band recombination models. The Fermi-Dirac statistics for calculation of carrier transport within non-parabolic conduction band has been used in present analysis[16–22].

2. SIMULATION AND ANALYSIS

2.1 Dark Current Analysis

Present study based on numerical simulation includes semiconductor continuity equations for holes and electrons and Poisson's equations. The semiconductor continuity equation and Poisson's equation for electrons and holes, respectively:

$$\frac{\partial n}{\partial t} = \frac{1}{q}\nabla J_n + \left(G_n - R_n\right) \tag{1}$$

$$\frac{\partial p}{\partial t} = -\frac{1}{q}\nabla J_p + \left(G_p - R_p\right) \tag{2}$$

$$div\left(\varepsilon_s \nabla V\right) = \rho \tag{3}$$

where n and p symbols depict the electrons and holes density, while J_n and J_p represents electron and hole current densities. The electrons and holes generation rate is taken by symbol G_n and G_p, R_n and R_p represents recombination rates for electrons and holes. The q is electronic charge. V, the electrostatic potential, ε_s and ρ are the local permittivity and the local space charge density respectively. In present simulation the third dimension has been ignored by choosing z as unity.

Boltzmann transport theory have shown that the current densities (J_n and J_p in Eqns. (1) and (2)) the continuity equations may be approximated by a drift-diffusion model and can be expressed in terms of electric field and gradient in carriers concentrations consisting of drift and diffusion components of carriers and given as under Boltzmann's assumption:

$$J_p = q\mu_p pE + qD_p \nabla p \tag{4}$$

$$J_n = q\mu_n nE - qD_n \nabla n \tag{5}$$

where μ_n and μ_p are the low field analytic mobilities dependent on doping and temperature of the electrons and holes respectively and D_n and D_p are diffusion coefficients and given as

$$D_n = \frac{kT}{q}\mu_n \tag{6}$$

$$D_p = \frac{kT}{q}\mu_p \tag{7}$$

The total dark current under biasing condition has been modelled by taken into account major current components as:

(i) The minority charge carriers diffuse from the neutral p and n regions of each hetero junctions producing diffusion current.

(ii) The generation recombination of charge carrier in the depletion region at the p -n junction is responsible for drift current.

(iii) The tunnelling of charge carriers across the p-n hetero interface produces tunnelling current.

Thus, the total dark of the proposed structure is combination of all above major current components and is[16-20]

$$J_{DARK} = J_{DIFF} + J_{GR} + J_{TUN} \tag{8}$$

where J_{TUN} is the tunnelling current component consist of probability of two types of tunnelling probability mechanisms i.e. direct band to band (BBT) and trap assisted tunnelling (TAT) and given as:

$$J_{TUN} = J_{BBT} + J_{TAT} \tag{9}$$

here J_{BBT} is the tunnelling current arises due to influence of local electric field which causes local band bending to allow electrons to tunnel, by internal field emission, from valance band into the conduction band and J_{TAT} is the trap assisted tunnelling current density and given as:

$$J_{TAT} = \frac{q^3 m_0 m^* EM^2 N_T G_T}{8\pi\hbar^3\left(E_g - E_T\right)} \exp\left(-\frac{4\sqrt{2m_0 m^*\left(E_g - E_T\right)^3}}{3q\hbar E}\right) \tag{10}$$

where E is the local electric field, m_0 and m^* are the rest and effective masses of the carriers, E_g and E_T are energy bandgap and trap energy states, N_T and G_T are trap density and trap degeneracy factor. M^2 is the matrix element associated with the trap potential.

3. SPECTRAL RESPONSE

The quantum efficiency is the figure of merit for photodetector technology. Quantum efficiency depicts the rate of conversion of photons (incident on photodetector of appropriate wavelength) into electron-hole pairs and dependent on the absorption coefficient of the materials. The absorption

of incident light at multilayer hetero-interface can be defined through matching of electric field at each interface with having constant refractive indices of each layer. The absorbed photons split into electron-hole pair (EHP) and inter diffusion process of EHP at each hetero-interfaces encourages crosstalk effects within the multilayer structure. Basically crosstalk effect can be modelled through three essential mechanisms[22-24].

a. Electrical crosstalk
b. Radiative coupling
c. Transmission of MWIR radiation through the MWIR absorbed structure

Coussa[22], *et. al.* proposed a model for dual waveband structures, considering radiative coupling to demonstrate the cross-talk effect in dual band photodetector. The basic mechanism of radiative coupling involve detection of EHP in LW band when MW radiation is active i.e. simply generation of electron-hole pairs (EHP) in MW band under incident MW wavelength.The generated electron recombine with the holes in MW band, giving photon of higher energy w.r.t to MW radiation. The higher energy re-emitted photons can be observed in LW band in form of EHP under the no radiation or dark condition. The probability of re-emitted photon absorption in LW band depends on radiative recombination efficiency in MW band. The crosstalk associated with dual band IR detector is simply dependent on the separation between MW and LW diodes. To minimise the crosstalk effect a thin barrier layer sandwiched between MW and LW diodes. The barrier layer thickness parameter is very important factor for reducing dark current due to crosstalk of carriers, associated with detectors, in turn quantum efficiency enhancement. In the proposed structure the effect of radiative coupling has been minimised by optimising the thickness of barrier layer between back-to-back diode.

The quantum efficiency of dual band infrared detector based on HgCdTe is the figure of merit for prediction of spectral performance. The quantum efficiency has been analysed with the multilayer approach, where electric field should match at each hetero-interface. The quantum efficiency of the dual band detector is dependent on reflection coefficients, transmission coefficients and absorption coefficient. The generation of electron-hole pair (EHP) due to absorption of incident light has been calculated as

$$G = \eta_0 \frac{P\lambda}{hc} \alpha e^{-\alpha y} \tag{11}$$

where P is the incident ray intensity responsible for absorption, η_0 is the internal quantum efficiency. y is the distance from the source, λ the incident wavelength, α is the absorption coefficient and is given as:

$$\alpha = \frac{4\pi}{\lambda} k \tag{12}$$

where k represents imaginary refractive indices for different layers. The different refractive index associated with different mole-fraction of the MCT layers have been used in present analysis. The spectral response in terms of photocurrent has been calculated with the help of absorption coefficient. With the help of Chu's model[25-27] imaginary part of the optical index (k) of refraction has been calculated.

4. RESULTS AND DISCUSSION

A physics based numerical model has been developed based on the historical dual band structure fabricated by Reine[13], *et. al.*, consisting of p/n/n/N/P with different mole fraction of five layers of MCT for simultaneous operation at 77 K at MW and LW windows shown in Fig. 1(a). The electrical and optical characterisation results based on the numerically developed model has been calibrated with the experimental results reported by Reine[13], *et. al*. The numerical model has been optimised and validated against the experimental results first, the rigorous analysis has been carried out for study of different physical mechanisms including different physics based model associated with the device structure. The simulation study has been carried out for understanding the electrical and optical behaviour of the structure.

Figure 1(b) depicts the simulated energy band with different location of conduction and valence band along with interfacial spikes. The discontinuities at each hetero-interfaces support good by Anderson theory for hetero structures. To restrict diffusion of LW carriers to MW band or MW carriers to LW band, an n-type MCT layer sandwiched between MW and LW absorber layers. The sandwiched n-type layer creates barrier for MW and LW carriers and help to reduce the crosstalk effect within two bands. The barrier height depends on barrier layer thickness and mole fraction of HgCdTe material. The crosstalk coupling from MW to LW and vice versa has been analysed in present study.

Figure 2 illustrates the numerically simulated dark current-voltage characteristics of the LWIR detector at different temperatures. The reverse dark current magnitude increases with the rise in the temperature. The effect can be concluded in terms of the generation-recombination component of the current. In the I-V computation, all the dark current components, i.e. diffusion, generation-recombination, trap assisted tunnelling and band to band tunnelling components have been taken into account. At 77 K temperature the dark current is low enough

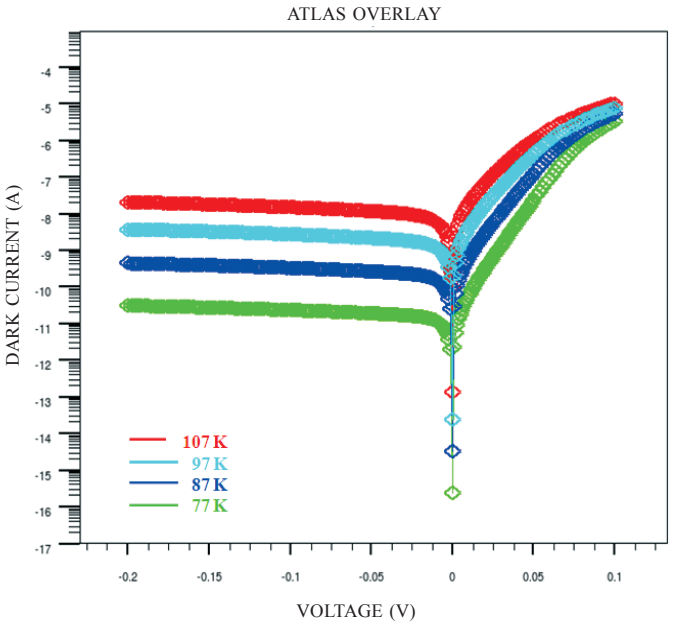

Figure 2. Variation of dark current of LWIR detector with reverse bias voltage at different temperature.

($\sim 5\times10^{-10}$ A), as the temperature increases the current increases with one order i.e. 10. It is clear from the graph for increase in temperature with 10 K, current increase with order of 10 under low reverse bias. Under low to moderate reverse bias all the curves at different temperatures show similar fashion and remain constant. The exponential increase in dark current has been observed under forward bias condition. The computation of dark current has been carried out by inclusion of diffusion, GR, TAT and BTB components in present study. The different dark current components results (not shown here) illustrate the G-R component of dark current dictate the dark current under low reverse bias, while TAT component of dark current shows negligible influence under same biasing. The higher potential barrier reduces the tunnelling phenomena at the hetero-interface. Hence the total dark current of LW detector is decided by generation-recombination (G-R) component of current under reverse bias condition.

The total dark current especially LW infrared detector contributed by diffusion, generation recombination, trap assisted tunnelling and band-to-band tunnelling components with applied voltage. We have applied our proposed analytical model[27] to estimate the dark current of LWIR detector under biasing condition at 77 K operation. The numerically simulated results based on numerical model are supporting the results obtained on the basis of analytical model of current, not shown here (please check [ref 27]). The total resistance-area product increases linearly in moderate and low reverse bias voltage upto zero reverse bias, showing linear dependence of total resistance-area product on reverse bias voltage in 105 Ω-m^2 -106 Ω-m^2 range of total dynamic resistance. The total resistance-area product has the maximum value of 106 Ω-m^2 near zero bias voltage.

Figure 3 elaborates the comparison between dark, photo and incident source currents. The incident light Intensity has been assumed constant during optical characterisation of the dual band IR detector. The curve shows overlapping of dark, photo and incident source currents for the incident waveband in 2 μm - 10 μm. The overall dark current of dual band detector for waveband 0 μm - 2 μm is almost negligible and increase exponentially under operative waveband and biasing conditions. Under operative wavelength range MW and LW of dual band photodetector, the dominant reflection at front surface, back surface and side wall reflection have been considered and computed by Fresnel's relations. So far the device is designed and coupled with source such that the maximum absorption occurs within the device. The anti-reflective (AR) coating, which relies on destructive interference of reflected photons, has been used to reduce the overall reflection coefficient of the incident light on the device. The photocurrent curve depict rapid fall beyond 10.34 μm, the cut off wavelength of LW diode.

Quantum efficiency of dual band detector has been shown in Fig. 4 at 77 K. The quantum efficiency of each photodiode has been computed separately for MW and LW bands. The quantum efficiency of MW detector is high at 2 μm - 2.5 μm wavelength range, constant at 2.5 μm to 4 μm wavelength range and reduces linearly upto its cutoff operative wavelength which is 4.5 μm. The maximum efficiency shown by MWIR detector is 95 per cent obtained at nearly 3 μm wavelength. Quantum efficiency exhibit by LW detector is comparatively low with respect to MW detector and shown almost constant under whole operative wavelength (4 μm - 10.6 μm) under biasing condition. The maximum quantum efficiency of LW detector has been obtained 74.5 per cent. The region crossing LW quantum efficiency curve by the MW quantum efficiency curve (from wavelength region 4 μm - 4.8 μm) depicts the crosstalk effect in the Fig. 4. The design of experiments (DOE) has been run to optimise the thickness of barrier layer to reduce crosstalk i.e. to prevent re-emitted photon from MW band to absorb in LW band. In present analysis the crosstalk has been analysed by taking ratio of LW band current to MW band current under condition when MW diode illuminated and LW radiation is off.

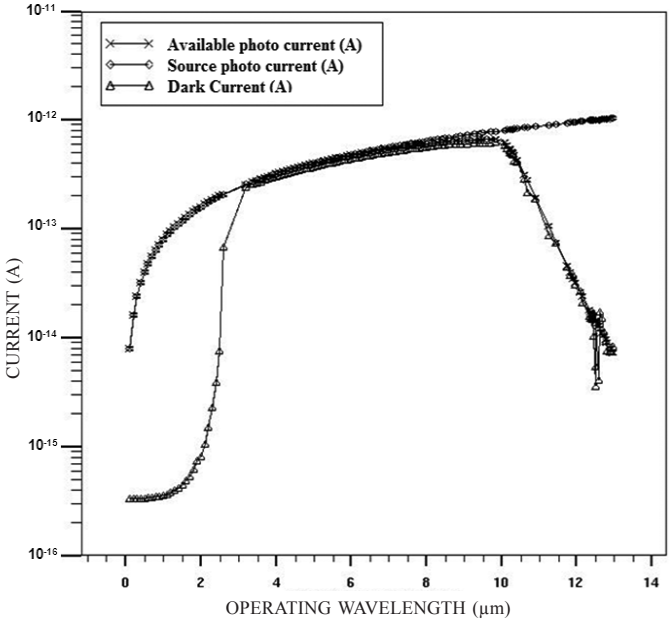

Figure 3. Variation of different currents with operating wavelength.

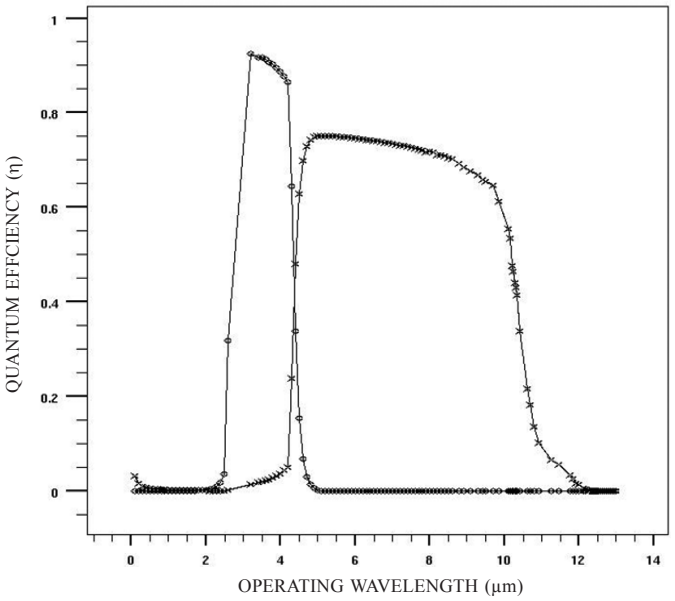

Figure 4. Variation of theoretically computed quantum efficiency with wavelength.

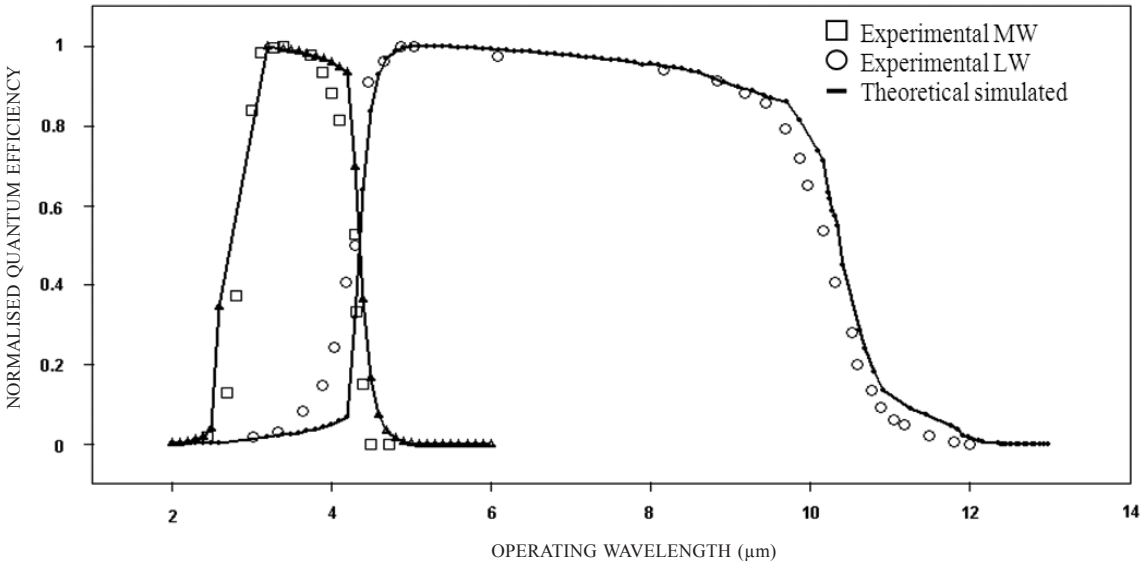

Figure 5. Variation of normalised quantum efficiency with operating wavelength.

The comparisons between theoretically computed result and reported experimental results[13] have been contrasted as shown in Fig. 5. The common electrical contact's dimension in the back to back diodes play significant role in the calculation of quantum efficiency. Quantum efficiency changes significantly with the minor changes in dimension of shorting contact. The MW quantum efficiency curve shows cut off wavelength 4.5 μm while for LW quantum efficiency it is 10.4 μm. The computed optical crosstalk is less than 3.5 per cent is which reasonable against the experimentally reported crosstalk (>4 per cent) in the wavelength region 4 μm - 4.8 μm. The optical crosstalk has been minimised in present proposed model by choosing appropriate optimum parameters for barrier layer. The theoretically computed relative quantum efficiency shows better results in terms of reduce crosstalk and improved cutoff wavelength for each back to back MW/LW photodetectors against the experimental results for the same. The exact comparisons of theoretically simulated and experimentally reported results are as shown in Table 1.

Table 1. Comparison of simulated and experiment data

Parameters	MW detector		LW detector	
	Computed	Experiment	Computed	Experiment
λ_{cutoff} (μm)	4.5	4.29	10.4	10.33
QE (η)	95%	79%	74.5%	67%

5. CONCLUSIONS

The performance analysis of simultaneous MCT dual band photodetector for operation wavelength MW/LW wave band has been predicted in present work. For two colors back to back photodetectors structure for simultaneously detection application has been designed. The parameters has been optimised to achieve better performance. The theoretical proposed model includes solution for decoupled semiconductor continuity, transport and Poisson's equations and has been solved to understand the underneath physics of transport of carrier's in the dual band detector. The results obtained on the basis of theoretical computations explained successfully all the inside physical phenomenon accurately and are supported by the experimental results. The crosstalk effect has been minimised in present study and further reduction in crosstalk is possible by choosing more optimum parameters for the barrier layer between MW and LW detector. The dark current is higher in LW detector as compared to MW detector hence the quantum efficiency is high for MW detector in dual band detection application under radiative conditions. The proposed theoretical model can be helpful to design engineers for developing MCT based dual band and multiband simultaneous infrared detectors.

REFERENCES

1. Rogalski. Competitive technologies of third generation infrared photon detectors. *Opto-Electronics Review*, 2006, **14**(1) 84-98.
` doi: 10.2478/s11772-006-0012-2
2. Vallone, M.; Goano, M.; Bertazzi, F.; Ghione, G.; Wollrab, R. & Ziegler, J. Modeling photocurrent spectra of single-color and dual-band HgCdTe photodetectors: Is 3D simulation unavoidable? *J. Electron. Mate.*, 2014, **43**(8). doi: 10.1007/s11664-014-3252-9
3. Blazejewski, E.R.; Arias, J.M.; Williams, G.M.; McLevige, W.; Zandian, M. & Pasko, J. Bias-switchable dual-band HgCdTe infrared photodetector. *J. Vac. Sci. Technol. B*, 1992, **10**, 1626-1632.
doi: 10.1116/1.586259
4. Reine, M.B.; Norton, P.W.; Starr, R.; Welier, M.H.; Kestigian, M. & Musictant, B.L. Independently accessed back-to-back HgCdTe photodiodes: A new dual-band infrared detector. *J. Electronic Mater.*, 1995, **24** (5), 669-679.
doi: 10.1007/BF02657977
5. Patten, E.A.; Goetz, P.M.; Vilela, M.F.; Olsson, K.; Lofgreen, D.D.; Vodicka, J.G. & Johnson, S.M. High performance MWIR/LWIR dual-band 640*480 HgCdTe/

Si FPAs. *J. Electronic Mater.,* 2010, **39**(10),2215–2219. doi: 10.1007/s11664-010-1294-1

6. Rajavel, R.D.; Jamba, D.M.; Jensen, J.; J.; Wu, O.K.; Beau, C.; Wilson, J.; Patten, E.; Kosai, K.; Johnson, J.; Rosbeck, J.; Goetz, P. & Johnson, S. Molecular beam epitaxial growth and performance of integrated two-color HgCdTe detectors operating in the mid-wave infrared band. *J. Electronic Mater.*, 1997, **26** (6), 476-481. doi: 10.1007/s11664-997-0180-y
7. Mitra, P.; Barnes, S.L. & Case, F.C. MOCVD of bandgap-engineered HgCdTe p-n-N-P dual-band infrared detector arrays. *J. Electronic Mater.*, 1997, **26** (6), 488-492. doi: 10.1007/s11664-997-0181-x
8. Rajavel, R.D.; Jamba, D.M.; Wu, O.K.; Jensen, J.E.; Wilsonb, J.A.; Patten, E.A.; Kosai, K.; Goetz, P.; Chapman, G.R. & Radford, W.A. High performance HgCdTe two-color infrared detectors grown by molecular beam epitaxy. *J. Crystal Growth* , 1997, **175/176**, 653-658. doi: 10.1016/S0022-0248(96)01200-6
9. Parish, G.; Musca, C. A.; Siliquini, J. F.; Antoszewki, J.; Dell, J. M.; Nener, B. D.; Faraone, L. & Gouws, G. J. A monolithic dual-band HgCdTe infrared detector structure. *IEEE Electron Device Lett.*, 1997, **ED-18** (7), 352-354. doi: 10.1109/55.596934
10. Rajavel, R.D.; Jamba, D.M.; Jensen, J.E.; Wu, O.K.; Brewer, P.D.; Wilson, J.A.; Johnson, J.L.; Patten, E.A.; Kosai, K.; Caufield, J.T. & Goetz, P.M. Molecular beam epitaxial growth and performance of integrated multispectral HgCdTe photodiodes for the detection of mid-wave infrared radiation. *J. Crystal Growth*, 1998, **184/185**, 1272-1278. doi: 10.1016/S0022-0248(98)80264-9
11. Jozwikowski, K. & Rogalski, A. Computer modeling of dual-band HgCdTe photovoltaic detectors. *J. Appl. Phys.*, 2001, **90**(3), 1286-1291. doi: 10.1063/1.1380989
12. Tissot, J.L. Advanced IR detector technology development at CEA/LETI. *Infrared Phys. Technol*., 2002, **43**, 223-238. doi: 10.1016/S1350-4495(02)00143-3
13. Reine, M.B.; Hairston, A.; Dette, P.O.; Tobin, S.P.; Smith, F.T.J. & Musicant, B.L. Simultaneous MW/LW dual band MOVPE HgCdTe 64×64 FPAs. *In* Proceedings of SPIE, 1998, **3379**, 200-212. doi: 10.1117/12.317588
14. ATLAS User's manual, device simulation software, SILVACO international, santa clara, CA 95054.
15. Sharma, B.L. & Purohit, R.K. Semiconductor heterojunctions, (Newyork: Pergamon Press, USA 1974).
16. Saxena, P.K. & Chakrabarti, P. Computer modeling of MWIR single heterojunction photodetector based on mercury cadmium telluride. Infrared Physics & Technology, 2009, **52**, 196-203. doi: 10.1016/j.infrared.2009.07.009
17. Saxena, P.K. Modeling and simulation of LWIR photodetector based on mercury cadmium telluride. *Infrared Phys. Technol.*, 2011, **54**, 25-33. doi: 10.1016/j.infrared.2010.10.005
18. Bellotti, Enrico & Orsogna, Danilo D. Numerical analysis of HgCdTe simultaneous two-color photovoltaic infrared detectors. *IEEE J. Quantum Electr.*, 2006 **42**(4), 418-426. doi: 10.1109/JQE.2006.871555
19. Gumenjuk-Sichevskaya, J.V. & Sizov, F.F. Currents in narrow-gap photodiodes. *Semicond. Sci. Technol*, 1999, **14**, 1124-1131. doi: 10.1088/0268-1242/14/12/320
20. Yang, R. Q.; Sweeny, M.; Day, D. & Xu, X. M. Interband tunnelling in heterojunction tunnel diodes. *IEEE Trans. Electron. Devices*, 1991, **ED-38**, 442–446. doi: 10.1109/16.75152
21. Ashley, T.; Dean, A. B.; Elliot, C. T.; Houlton, M. R.; McConville, C. F.; Tarry, H. A. & Whitehouse, C. R. Multilayer InSb diodes grown by molecular beam epitaxy for near ambient temperature operation. *In* Proceedings of SPIE, 1990, **1361**, 238–245. doi: 10.1117/12.24426
22. Coussa, R.A.; Gallagher, A.M.; Kosal, K.; Pham, L.T.; Pierce, G.K.; Smith, E.P.; Venzor, G.M.; Delyon, T.J.; Jensen, J.E.; Nosho, B.Z.; Roth, J.A. & Waterman, J.R. Spectral crosstalk by radiative recombination in suquential-mode, dual mid-wavelength infrared band HgCdTe detectors. *J. Electronic Mater.*, 2004, **33** (6), 517-525. doi: 10.1007/s11664-004-0040-y
23. Tian, Y.; Zhang, B.; Zhou, T.; Jiang, H. & Jin, Y. Numerical analysis of the detectivity in n+-n-p and p+-p-n GaInAsSb infrared detectors. *Solid-State Electron.*, 1999, **43**, 1879–1891. doi: 10.1016/S0038-1101(99)00049-0
24. Tian, Y.; Zhou, T.; Zhang, B.; Jiang, H. & Jin, Y. Effect of material parameters on quantum efficiency of GaInAsSb detectors. *Solid State Electron.*, 1999, **43**, 625–631. doi: 10.1016/S0038-1101(98)00294-9
25. Chu, J.; Mi, Z. & Tang, D. Intrinsic absorption spectroscopy and related physical quantities of narrow-gap semiconductors $Hg_{1-x}Cd_xTe$. *Infrared Phys*., 1991, **32**, 195-211. doi: 10.1016/0020-0891(91)90110-2
26. Chu, J.; Mi, Z. & Tang, D. Band to band absorption in narrow-gap $Hg_{1-x}Cd_xTe$ semiconductors. *J. Appl. Phys*., 1992, **71**, 3955-3961. doi: 10.1063/1.350867
27. Saxena, P.K. Numerical simulation of dual-band HgCdTe photodetector. Presented at the fifteen international workshop on the physics of semiconductor devices. Proceeding IWPSD-2009, 587-590.

CONTRIBUTORS

Dr Praveen Kumar Saxena received the Bachelor and Masters in Physics from University of Lucknow and PhD in Electronics Engineering from Indian Institute of Technology (IIT), Banaras Hindu University, India. He started working on Infrared detectors based on Narrow bandgap materials during 2005. Since then he is continuing for modelling and designs of different IR technologies. His research area includes infrared detectors (photoconductive, photovoltaic, QWIP, SLS type I & II) and MEMS especially on cantilever based applications. He works on all semiconductor technologies based on organic and inorganic semiconductor materials.

Appendix

The numerical simulation includes the following set of formulae for computation of different physical parameters:

The Energy band gap for $Hg_{1-x}Cd_xTe$ material dependent on mole fraction x and given as

$$E_g = -0.302 + 1.93x - 0.81x^2 + 0.832x^3 + 5.35\times10^{-4}(1-2x)T \quad (13)$$

Electron affinity for MCT material is given as

$$\chi = 4.23 - 0.813\left(E_g - 0.083\right) \quad (14)$$

The mobility of electron is

$$\mu_n = 9\times10^8\left(\frac{0.2}{x}\right)^{7.5} T^{-2\left(\frac{0.2}{x}\right)^{0.6}} \quad (15)$$

Effective mass ratio of electrons and holes are

$$\frac{m_n^*}{m_0} = \left[-0.6 + 6.333\left(\frac{2}{E_g} + \frac{1}{E_g + 1}\right)\right]^{-1} \quad (16)$$

$$\frac{m_p^*}{m_0} = 0.55 \quad (17)$$

Dielectric coefficient

$$\varepsilon_s = 20.5 - 15.5x + 5.7x^2 \quad (18)$$

The effective Richardson constant is defined as

$$R^* = \frac{4\pi q k^2 m^*}{h^3} \quad (19)$$

For MCT material, the temperature dependent real refractive indices empirical formula for mole fraction range from 0.276 to 0.540 and temperatures range from 4.2 K to 300 K is given by,

$$n^2(\lambda, T) = A + \left(\frac{B}{1-(\frac{C}{\lambda})^2}\right) + D\lambda^2 \quad (20)$$

where

A=13.173-9.852x+2.909x^2+(300-T)10^{-3}

B=0.83-0.246x-0.0961x^2+8(300-T) 10^{-4}

C=6.706-14.437x+8.531x^2+7(300-T)10^{-4}

D=1.953e-4-0.00128x+1.853e-4x^2

The imaginary part of refractive indices is dependent on absorption and computed as

$$k = \frac{\lambda}{4\pi}\alpha \quad (21)$$